



Supplementary Materials for  
**Neuroethology of natural actions in freely moving monkeys**

Francesca Lanzarini *et al.*

Corresponding author: Luca Bonini, [luca.bonini@unipr.it](mailto:luca.bonini@unipr.it)

*Science* **387**, 214 (2024)  
DOI: [10.1126/science.adq6510](https://doi.org/10.1126/science.adq6510)

**The PDF file includes:**

Materials and Methods  
Supplementary Text  
Figs S1 to S12  
Table S1  
References

**Other Supplementary Material for this manuscript includes the following:**

Movies S1 to S4

## Materials and Methods

### Animals

Two male rhesus macaques (*Macaca mulatta*: Mk1, 8 years, and Mk2, 10 years) were used in the experiments. The facilities provide cage size exceeding the requirements of Italian and European regulations, and daily access to an enriched environment including wooden structures and various toys. The experimental protocols complied with the European law on the humane care and use of laboratory animals (Directive 2010/63/EU), were approved by the Veterinarian Animal Care and Use Committee of the University of Parma and authorized by the Italian Ministry of Health.

### Apparatus and behavioral paradigm

The two monkeys were trained to autonomously enter a primate chair and to be transported in the laboratory. Both monkeys were chronically implanted with a titanium head post (Crist Instruments, Hagerstown, MD, USA) to perform head-fixed sessions. Once fully trained to have their head fixed and receive solid and liquid rewards, they were trained to perform forelimb and mouth motor actions under conventional laboratory conditions at the center of the NeuroEthoRoom (NER), which allowed us to monitor the animals' behavior with a multicamera system. The NER is a transparent Plexiglas enclosure (W x H x D, 205 x 205 x 180 cm), surrounded by a system of 8 color cameras, which enabled us to record the macaque behavior at 50 Hz throughout the sessions, synchronized with the neural data acquisition system (see below).

The experimental session and data acquisition included two steps: first, neuronal activity and behavior were recorded in a restrained context (RC), in which the monkey was head-fixed in the primate chair at the center of the NER; next, in the second part of the recording session, the same cells and the monkey's behavior were recorded in a freely moving context (FMC), by leaving the monkey free to move in the NER enriched with a wooden structure and a rope for climbing, seeds and small pieces of food on the floor for foraging, and fruit morsels hanged on hooks lowered from above through transparent wires, allowing the monkey to catch them on the fly.

In the RC, we could study neuronal activity while monkeys were performing different types of actions.

Reaching-grasping actions. Starting with its hand from an initial position close to its body, the monkey reached and grasped a piece of food positioned on a tray and suddenly presented by the experimenter lifting a shutter within the animal's reach; the monkey grasped the food with a spontaneously selected grip (typically a side grip, performed by opposing the thumb with the lateral part of the index finger) and brought it to the mouth to eat. For each action at least ten trials were collected, interleaving trials performed with the monkey's right and left hand.

Mouth actions. The monkey was given directly in its mouth the same type of food morsels used for the reaching-grasping actions by the experimenter using a stick, to test biting of the food without the use of the hand. Furthermore, the monkey was given some drops of juice with a plastic syringe, which it sucked and drunk without the use of the hands. Also in these cases, at least 10 trials for each action were collected.

At the end of the testing phase in the RC, the monkey's head was released, and the animal in the primate chair was moved out of the cage temporarily (approximately 10 minutes) while the NER was enriched by the experimenters with the items needed for the subsequent phase of the session. Next, the monkey was allowed to enter the NER directly from the primate chair, through

a vertical sliding door in the frontal part of the NER. In the FMC, the monkey could spontaneously explore all the volume of the NER and express any possible type of behavior with no restrictions. In order to elicit at least the same actions that could be tested in the RC, the experimenter periodically offered juice to the monkey using the same syringe employed in the RC, introducing it through small apertures in the Plexiglass walls, and pieces of food with the same stick used in RC, to elicit biting when taking food directly with its mouth. Additionally, it could forage from the ground and catch fruit morsels lowered into the NER through transparent wires hanging from the ceiling. In addition, many other different actions spontaneously occurred (e.g. scratching, climbing, yawning, walking, etc.), with considerable variability in their frequency across sessions, as they entirely depended on the monkey's willingness to produce them.

### Surgical procedures

Each monkey underwent three surgeries: first, they received the titanium head-post, and subsequently each animal was implanted with a variable number of 32-channel floating microelectrode arrays (FMA, Microprobes for Life Science, Gaithersburg, MD, USA) in both hemispheres at different times. In particular, first we implanted the left hemispheres (n = 4 probes in Mk1; n = 6 in Mk2, of which 5 were used for this study, Fig. S1A) and then the right hemispheres (n=6 probes in both monkeys, Fig. S1A). A customized recording chamber equipped with a regularly spaced grid was secured to the skull with bone screws and dental cement, acting as a connector block for 32 channel Omnetics connectors (Fig. S1B). The chamber housed the cables coming from the arrays and was partially filled with liquid dental cement, which rapidly solidified isolating its inner part from the outside, and then further protected with QuickCast silicone. The Omnetics connectors were locked to the grid by a further plastic block screwed on top of them, and finally the chamber was closed with a cover screwed to it. During neural data logging, a further, larger protective cover was fixed and screwed on top of the chamber, allowing to house and protect the neural data loggers and the battery pack (Fig. S1B and C).

All surgeries were carried out under general anesthesia, in aseptic conditions, followed by postsurgical pain medications. Animals were prepared for the anesthesia by administering atropine (0.03 mg/kg) 15 minutes prior to the induction of anesthesia with ketamine (4.5 mg/kg) and medetomidine hydrochloride (0.05 mg/kg). Anesthesia was then maintained via inhaled isoflurane (IsoFlo, 100% p/p). A multiparameter monitor allowed us to constantly control heart rate and ECG, SPO2 and respiration parameters, blood pressure and body temperature. Hydration was maintained by continuous infusion of saline solution (5 ml/kg/h). Before the implantation of electrode arrays, the animals were prophylactically treated with phenobarbital with progressively increasing dose (1-6 mg/kg, PO), starting from 1 week before the surgery and until 4 weeks post-surgery (fading out the dose over the last 2 weeks), to prevent seizures after probe implantation. At the end of each surgery, antibiotics (Benzylpenicillin Benzatin 25000 U.I./ml + Dihydrostreptomycin 100 mg/ml), dexamethasone (Soldesam, 0.15 mg/kg) and ketoprofen (Vet-Ketofen, 3 mg/kg) were administered for a variable number of days depending on the surgical procedure.

Electrode arrays were implanted by estimating the location and extent of the craniotomy with MRI-based reconstruction of the monkey skull. After opening the bone breach, the specific site of insertion was decided based on visible anatomical landmarks, particularly the superior and inferior arcuate sulci and the central sulcus. Our customized FMAs design includes two alternated electrode lengths (2.5 and 4 mm), which allowed us to explore different depths of the cortex. The customized plastic cover enables the communication of the logger with the transceiver, to keep the

synchronization of the recorded neural data with the video collected by the multicamera system, and ensuring the highest quality of the neural signal (Fig. S1D), as it does not need to be transferred via a radio frequency.

### Behavioral data acquisition and analysis

To combine the ethological study of animals' behavior with the neuronal recordings, we devised a transparent Plexiglass enclosure with minimal amount of metal, the NeuroEthoRoom (NER - see Fig. S1E), which allowed us to film the animal's behavior from multiple (n=8) cameras synchronized with the neural data.

The data were scored frame by frame (at 50 Hz resolution) using a dedicated software (BORIS) (21) by two independent observers with extensive training and experience with non-human primates in laboratory contexts (Fig. S1F), leveraging an ethogram specifically developed during the behavioral preparation of the animals for the recording sessions both in RC and FMC (Fig. S2). Considering the brain area of interest, we also marked separately forelimb actions performed with the left and right forelimb, ipsi- and contra-lateral to the recorded hemisphere, respectively. We generated an output for each session containing the timestamps related to all the behavioral point events.

Concerning the alignment point of each action, we selected a critical point constituting the transition between distinct motoric phases of each action (e.g. finger opening/closure during the various type of grasping, arm extension/flexion for steps during walking, mouth opening/closure in biting, drinking or yawning). This point is typically associated with a peak in somatosensory and/or proprioceptive feedback. For each transitive action defined in the ethogram (Fig. S2) the alignment point corresponds to the moment when a body part makes contact with the monkey's own body (scratching) or with an external object (all transitive hand and mouth actions, e.g. the food in biting, the syringe in drinking, the floor in each step of walking, etc.); for intransitive actions, such as yawning, the alignment point (i.e. maximal mouth aperture, Fig. S2) corresponds to the peak of proprioceptive feedback.

### Neural recording techniques

We simultaneously recorded from 128 channels distributed across 4 FMAs implanted in the lateral precentral cortex by mean of a wireless neural data logging system (RatLog-128, Deuteron technologies, Jerusalem, Israel). The recordings were performed with a bandpass filter set to 2-7000 Hz and a sampling rate of 32000 Hz on each channel. Signals were amplified, digitized, and stored locally, in a MicroSD memory card (64 GB). The logger was powered by an external battery (3.7V) directly connected with it and housed in the protective cover (Fig. S1B and C). The logger received from a transceiver a synchronization signal, consisting in a 50 Hz pulse of 5V generated by an external PC equipped with a National Instrument board. This signal was stored on the SD card together with the neuronal activity, and in parallel the same signal was fed to the SIMI Motion capture system (Simi Reality Motion Systems GmbH, Unterschleißheim, Germany) to act as a trigger for the acquisition of each frame of the video from all the 8 cameras, thereby enabling the synchronization of video and neuronal signals.

## Spike sorting and assessment of the recording stability

All formal analyses were carried out offline. The signal from all the recorded channels was band-pass filtered (300-6000Hz) and spike detection was performed with a negative threshold of 3 standard deviation from the mean signal of each channel. Detected spikes were then sorted using either an automated software (MountainSort) (23), setting “noise overlap” threshold at 0.20 for single units, or Plexon Offline Sorter (Plexon Inc). Since well-isolated single neurons were the primary target of this work, putative single unit were further scrutinized by manual curation using standard criteria. First, we discarded any unit identified by the automated software that exhibited a clearly non-physiological waveform. Second, we merged waveforms isolated in the same channel that exhibited the same waveform shape and ISI distribution but slightly different spike amplitudes distribution along the session, suggesting that they were indeed the same single unit occasionally clustered into separate ones because of drift in spike amplitudes during the recording (see Fig. S4 for final demonstration of single unit stability over time). Third, to exclude potential contamination with multiunit spikes, we checked whether the inter-spike interval (ISI) distribution of the extracted single units fulfilled the criteria of a refractory period longer than ~1 ms. The waveforms that were not clustered into a well-isolated and stable unit constituted the multiunit activity.

To assess the temporal stability of the isolation of single units, we extracted from each channel the waveform of all the N spikes in a 100-point clip (~3ms) centered on the spike minimum. The resulting Nx100 matrix underwent Principal Component Analysis (PCA) to reduce the waveform space to three dimensions. In this space, we calculated in one-minute bins the distance of the waveforms attributed to single units from those attributed to the multi-unit, taking the median of spike values in that minute for each principal component. The distances between single- and multi-units for each session were smoothed using a moving median (10 minutes), interpolated to align sessions of different durations, and normalized to the value of the first minute (see Fig. S4). All single units whose distance drifted in time toward the multiunit and merged with it or appeared/disappeared suddenly at a certain point during the session, were classified as unstable and excluded from all subsequent analyses (n=6, Mk1; n=3, Mk2).

## Analysis of firing features

For each neuron and in each of the two tested contexts (RC and FMC), we extracted a firing rate vector by binning spikes in 20 ms bins. Then, the average firing rate was calculated as the average across bins of the firing rate vector, and the maximum firing rate was calculated as the maximum across bins of the firing rate vector smoothed with a Gaussian filter ( $\sigma = 100$  ms). As an index of firing variability, we computed the Fano Factor by extracting a firing rate vector in 200 ms bins and calculating the ratio between the variance and average across bins. To analyze the possible relation and differences between these firing features in RC and FMC, we applied Wilcoxon Signed-rank test for paired samples comparisons and Spearman correlation analysis.

## Construction of peri-event histograms and analysis of neuronal tuning

In FMC the number of occurrences of each action cannot be controlled and varies considerably across sessions. Thus, for actions with a high number of occurrences, we randomly subsampled to a maximum of 20 occurrences for constructing the peri-event histograms and to analyze single neuron modulation. This was done both for visualization purposes and to mitigate possible false

positive bias in single neuron modulation due to oversampling of highly repetitive actions (e.g. steps). The dataset for evaluating single neuron modulations in FMC was pre-processed by binning the spikes of each neuron in non-overlapping 100 ms epochs within a time window centered on the alignment point of each action. The duration of the time windows was optimized for each action based on a tradeoff between the needs to capture the largest action unfolding period and the necessity to limit the overlapping between functionally linked behaviors occurring sequentially. The selected time windows relative to each event (considered at time 0) were:  $\pm 1$  s for bite and drink;  $-0.8/+0.5$  s for grasp, climb and step with either limb;  $\pm 2$  s for yawn and scratch. A one-way repeated-measure ANOVA was then applied to test for statistical differences among epochs in the time window related to each action, and considering a neuron as modulated for a given action if the ANOVA resulted in a significant main effect ( $\alpha=0.01$ ) and the neuron average firing rate in the time window was higher than 0.5 spk/s. This procedure was motivated by the fact that in the absence of a baseline, the null hypothesis was that if a neuron was not related to a given action, then its firing rate should not significantly change while that action was performed. Actions occurring less than 5 times in a session were considered as untestable in that session.

To compare single neuron modulations across the two contexts we employed a mixed ANOVA (within factor: epoch; between factor: context) carried out for each of the four actions occurring in both contexts (Bite, Drink, Grasp with contralateral and ipsilateral hand). For each action, a neuron was considered modulated if it exhibited a significant main effect of epoch and at least one significant post-hoc comparison ( $\alpha=0.01$ , Tukey-Kramer correction). For each action, if a neuron was modulated, we looked at the epoch-by-context post-hoc comparisons within each context, and the neuron was considered modulated in a context if at least one post-hoc comparison was significant. Finally, for each action, we investigated whether the modulations across RC and FMC were similar or different: a neuron was considered differently modulated ( $FMC \neq RC$ ) if there was a significant interaction between epoch and context and at least one significant context-by-epoch post-hoc comparison; otherwise, it was considered similarly modulated ( $FMC = RC$ ).

Sørensen-Dice coefficient. To evaluate the similarity in single-neuron tuning across the different actions during FMC, we calculated a variant of the Sørensen-Dice coefficient (SDC) for each pair of actions:

$$SDC_{AB} = \frac{2\tilde{N}_{AB}}{\tilde{N}_A + \tilde{N}_B}$$

where  $\tilde{N}_{AB}$  denotes the weighted number of neurons significantly tuned for both actions A and B, and  $\tilde{N}_A$  and  $\tilde{N}_B$  denote the weighted number of neurons significantly tuned for either action A and B, respectively, in sessions with sufficient occurrences for both actions. Each neuron was weighted with the degree of its tuning selectivity, i.e., one minus the fraction of actions the neuron was tuned for, such as the SDC between two actions “sharing” neurons tuned only for those two actions resulted higher than the SDC between two actions sharing neurons tuned for several other actions. In the case of yawn, that did never reach a sufficient number of occurrences in the same session with bite, catch food contra, rope climb and scratch, we estimated its SDC with those behavior by taking the average SDC of yawn with all the other available actions.

A hierarchical cluster analysis was applied to the distance matrix defined as 1 minus the SDC matrix; the corresponding dendrogram was constructed based on the Ward linkage criterion, and the SDC matrix was arranged accordingly (see Fig. 2C). Leaves within a branch were arranged according to their average distance to the nearest branches. Finally, we repeatedly shuffled tuning

labels across all neurons and actions (1000 times) to obtain a chance SDC distribution whose 95<sup>th</sup> percentile defined a significance threshold ( $\alpha=0.05$ ): all actions (or group of actions) showing a SDC higher than threshold were represented with the same color.

## Population analyses

### Neural population trajectories and alignment index

We quantified the similarity in the neural population codes among pairs of actions occurring in different contexts (Fig. 3D) by computing the residual variance obtained after projecting the neural trajectory associated to one action in one context (i.e. RC or FMC) onto the neural subspace of the same and any other action in the same and any other context (23, 44). To this purpose, first we calculated the soft-normalized firing rate of each neuron in a  $-0.8/+0.5$  s time interval relative to the alignment point of each action (five trials minimum). The spikes of each neuron were binned in 20-ms time windows, averaged across trials, smoothed with a Gaussian kernel ( $\sigma=60$  ms), and soft-normalized relative to the absolute maximum  $+5$  spk/s, to reduce the influence of low-firing neurons (45). We obtained eight matrices for Bite, Drink, Grasp with contralateral and ipsilateral hand in RC and FMC, each with dimensions  $T \times N$  ( $T$  being the number of time bins,  $N$  the number of neurons). For any pair of actions  $A$  and  $B$ , we applied PCA to the corresponding mean-centered data matrices  $X_A$  and  $X_B$ , obtaining the coefficients of the first five principal components  $V_A$  and  $V_B$  (five principal components typically captured nearly 90% of the total variance of a given action). Next, we evaluated the overlap or “alignment” of action  $A$  over action  $B$  by projecting the neural activity of  $A$  onto the principal components  $V_B$  and computing the residual variance normalized by the variance captured by the first five principal components  $V_A$ , as follows (45):

$$alignment_{AB} = \frac{tr(V_B^T cov(X_A) V_B)}{tr(V_A^T cov(X_A) V_A)}$$

The alignment index ranges from 0 (if neural subspaces are orthogonal) to 1 (if neural subspaces are perfectly aligned). We calculated the alignment index for any pair of actions, resulting in an alignment index matrix. Next, a hierarchical cluster analysis was applied to the distance matrix defined as 1 minus the symmetrized alignment matrix; the corresponding dendrogram was constructed based on the Ward linkage criterion, and the alignment matrix was arranged accordingly (see Fig. 3D-E).

The drawings of neural population trajectories were produced as follows. Given the neural activity matrices  $X$  of a given population (obtained as described above), we normalized them for the square root of their corresponding total variances to make the amplitude of the projected population trajectories comparable across behaviors (irrespective of the magnitude of their overall modulations), thus qualitatively reflecting the value of the alignment index (46). The population dynamics associated to each action in each context has been projected onto the first two PCs of every combination of action and context (Fig. S11).

### Neural decoding analysis

FMC Decoding. The FMC Decoding analysis was designed to determine if a decoder based on Support Vector Machine (SVM) model with linear kernel could classify various movements in the

FMC (Fig. 2F). For each session, we created balanced datasets randomly picking the same number of trials ( $\geq 10$ ) from each class of movement. To address significant original imbalances (e.g., step vs yawn), we repeated this random undersampling 10 times. The predictors were characterized as the temporal evolution of spike counts derived first from only single-units' activity and second from both single- and multi-units' activity. For every event, we identified the timestamp of the alignment point and proceeded to tally the spikes within a temporal window centered around this reference point. Following a symmetrical approach, we gradually introduced bins, two at a time with 50% overlap, extending the coverage to a maximum of (-1.0, +1.0) s in relation to the alignment point. This binning procedure was iterated for four different window lengths: [1.0, 0.5, 0.2, 0.1] s. After z-scoring, we projected the predictors onto the principal components explaining 90% of the variance, and we performed Leave-One-Out Cross Validation (LOOCV) for validating the SVM model. At the conclusion of all decoding sessions, the performances achieved during the tuning process and averaged across the 10 balanced datasets were compared and ranked to determine the optimal binning strategy capable of consistently delivering high performance across all sessions. The binning strategies were ranked according to their respective mean accuracies over the 10 partitions, and the top five appearing in all sessions were retained. The distances from the maximum mean accuracies in each session were then calculated and summed up. The strategy resulting in the minimum aggregate distance was identified as the winning strategy. The consensus favored the use of 0.5 s bins for both single-units decoding and single- combined with multi-units decoding. In our study, the entire range from -1.0 s to +1.0 s yielded the best overall performances for single unit decoding (Fig. 2F and Fig. S7). Conversely, when using both single- and multi-units, shorter dynamics (from -0.75 s to +0.75 s) resulted in superior performances, surpassing those obtained solely with single-units (Fig. S8 and Fig. S9).

Sliding Decoding. In the Sliding Decoding analysis, we explored the robustness of our decoder and how its performance evolves when considering predictor arrays not centered around the alignment points, but instead spanning through 5 seconds before and after these reference points. A nearly identical pipeline was employed for this analysis. We used the same responses from the previously defined 10 balanced datasets. The respective predictors, this time composed of only single unit activity, underwent iterative adjustments using a single spike count binning strategy, which was shifted in time by half the bin's dimension. The binning strategy for this study was chosen using the previously described ranking method, with the exception that dynamics exceeding 1 second were excluded. This adjustment aimed to enhance the temporal resolution for detecting relevant neural dynamics. The ranking method favored 0.2 s bins and a total coverage of 1.0 s. For each investigated interval, we conducted cross-validation using LOOCV, and averaged the accuracies obtained from the 10 balanced datasets. Finally, for each session, we plotted the mean accuracies for each time interval. Given the resulting bell-shaped curves (see Fig. 2G), we also sought to identify a specific time point where there is a notable variation in decoder performances. For this purpose, we searched for the elbow, i.e. the point where the curve visibly bends from low to high slopes, using the `knee_pt` function from MATLAB Central File Exchange on the smoothed profiles.

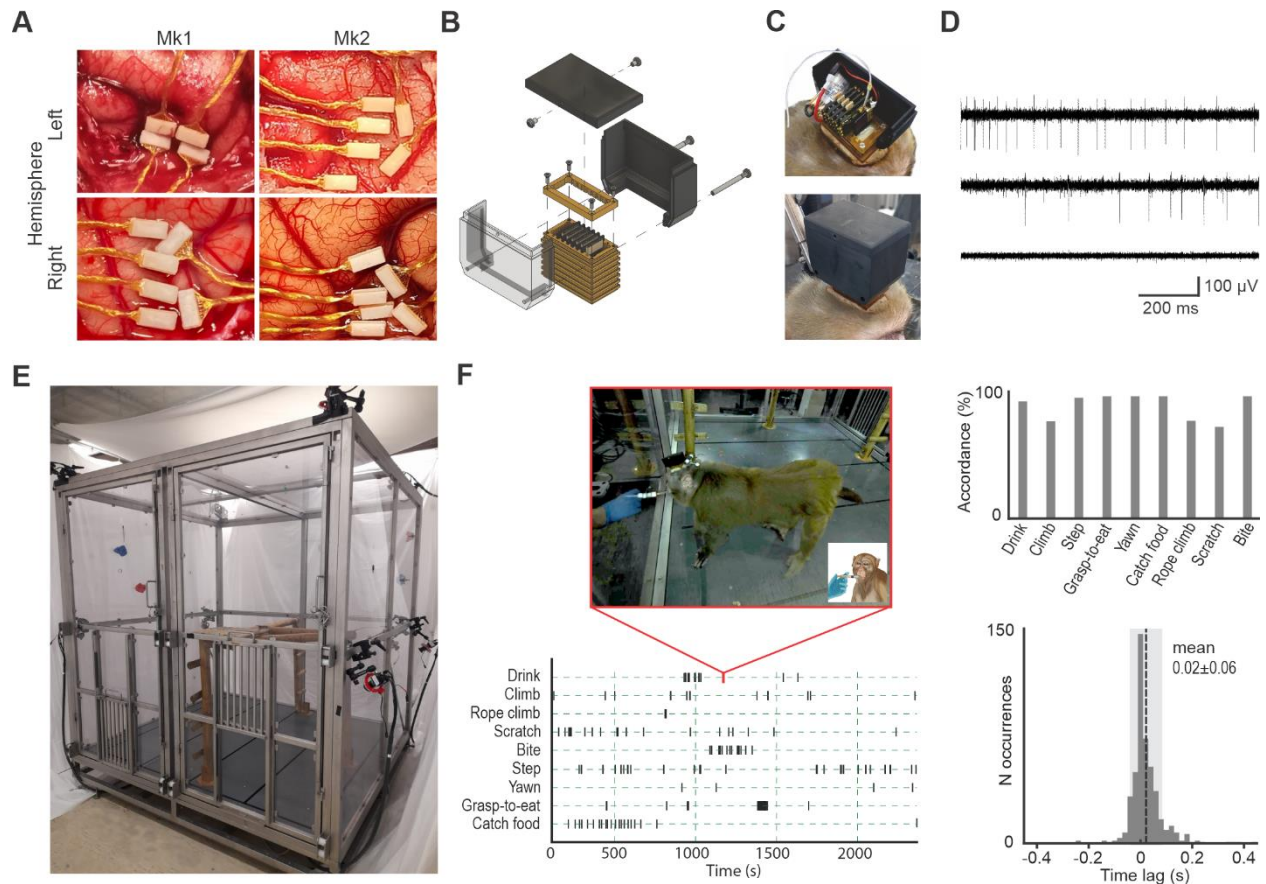
Cross-Context Decoding. To compare the generalization power of our decoder when trained with RC versus FMC data, a Cross-Context Decoding analysis was applied considering the four behaviors occurring in both contexts. Due to the inherently higher variability of the FMC data, we considered the grasp contra- and ipsi-lateral by merging grasp-to-eat and catch food trials (with a specific hand), to avoid making assumption on the grasping actions in FMC mostly similar to the




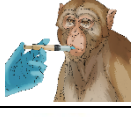






same actions in RC. Furthermore, this analysis was applied to only 9 sessions, because one did not contain a sufficiently large number of biting occurrences. With the new responses' arrangement, random undersampling was performed again to obtain a total of 20 different balanced datasets, 10 for RC and 10 for FMC. For this study specifically, only predictors containing both single- and multi-unit activity were tested. Using LOOCV, we trained the SVM model using one context dataset and validated it by either using the left-out element from the same context (intra-decoding) or by utilizing its corresponding event in the other context (inter-decoding). The process was repeated 10 times, one for each partition of the dataset, and the overall accuracies were averaged across these 10 repetitions. This resulted in a total of four training-validation sets combinations: RC→RC, FMC → FMC, FMC → RC, and RC → FMC. Similarly to FMC Decoding, various binning strategies were tested and ranked to determine the optimal spike count binning. The ranking method favored 0.5 s bins with a total coverage of 1.5s. The final four confusion matrices were generated by averaging the nine sessions confusion matrices for each training-validation combination (see Fig. 4A).

### Intracortical microstimulation experiments

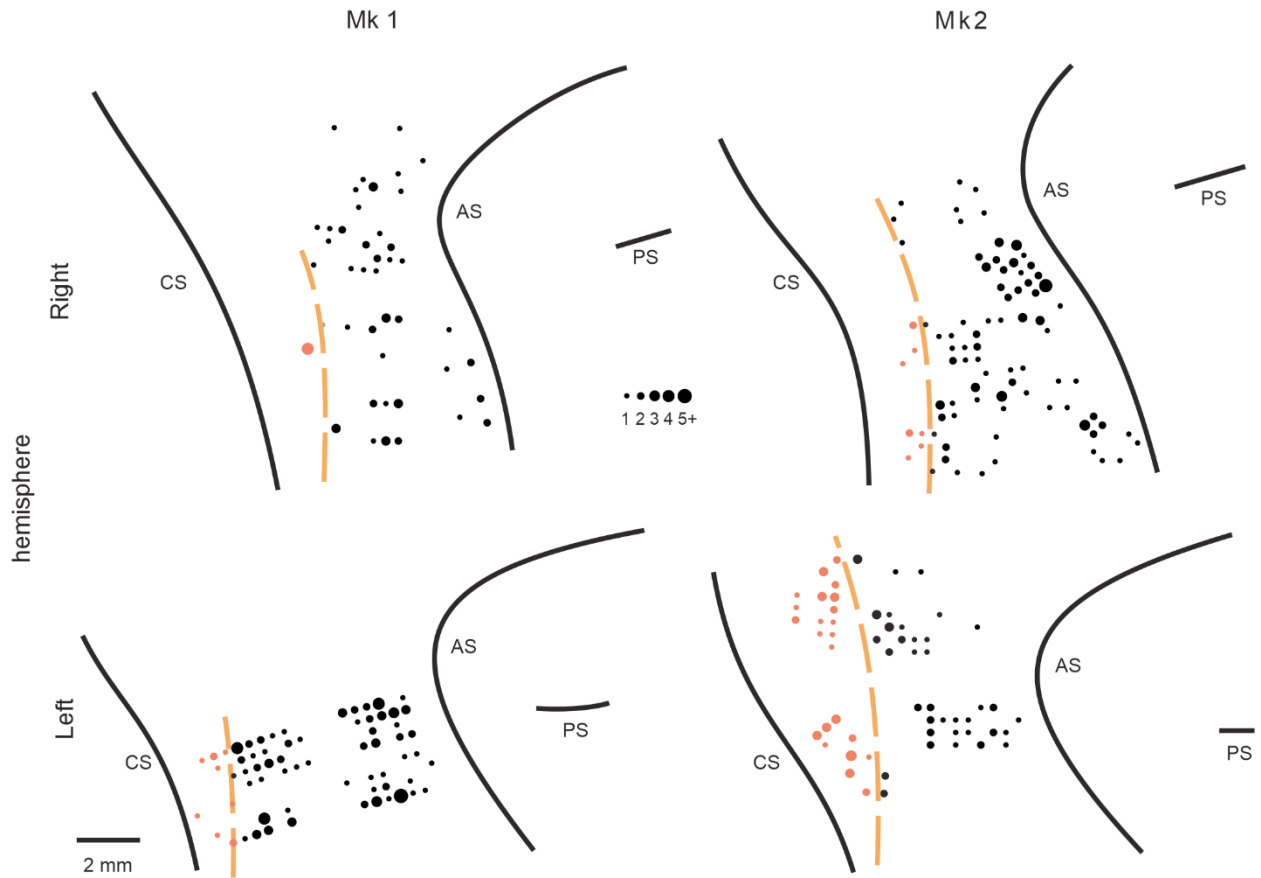
ICMS was performed in both monkeys during sessions distinct from the recording sessions. During each ICMS session, the experiments were conducted in RC, first with the monkey head-fixed, and then with the head free. Monopolar, biphasic trains of cathodic square wave pulses were delivered through a constant current stimulator (PlexStim, Plexon), with the following parameters: total train duration 500 ms, single pulse width 0.2 ms, pulse frequency 200 Hz, current intensity 100 $\mu$ A and 150 $\mu$ A. The same parameters were also applied with 50 ms trains, varying the current intensity to reach the lowest intensity threshold capable to elicit an observable movement, with the aim to identify the putative border between premotor and primary motor cortex. We monitored the current and voltage waveforms on an oscilloscope. At each site, ICMS was delivered when the monkey was quiet and relaxed; if the monkey performed voluntary movements before or during the stimulation, these were not considered to be the result of ICMS and the trial was repeated. Movements were considered to be evoked by ICMS when 2 experimenters, independently and repeatedly observing the animal during pulse delivery, identified the same movement or muscle twitch, consistent with previous studies (22, 47). All the experiments were also filmed and the ICMS results cross-checked offline by independent observers to achieve a more accurate description of the evoked effects. Effectors involved in movements elicited by ICMS were *mouth* (jaw or lips movements) and *face* (movements of any face portion different from jaw and lips), *hand* (movements of fingers and/or wrist), *hand-and-mouth* (movements of the two previous categories were observed simultaneously), and *axio-proximal* (neck/head, trunk or the upper part of the arm between the elbow and the shoulder).



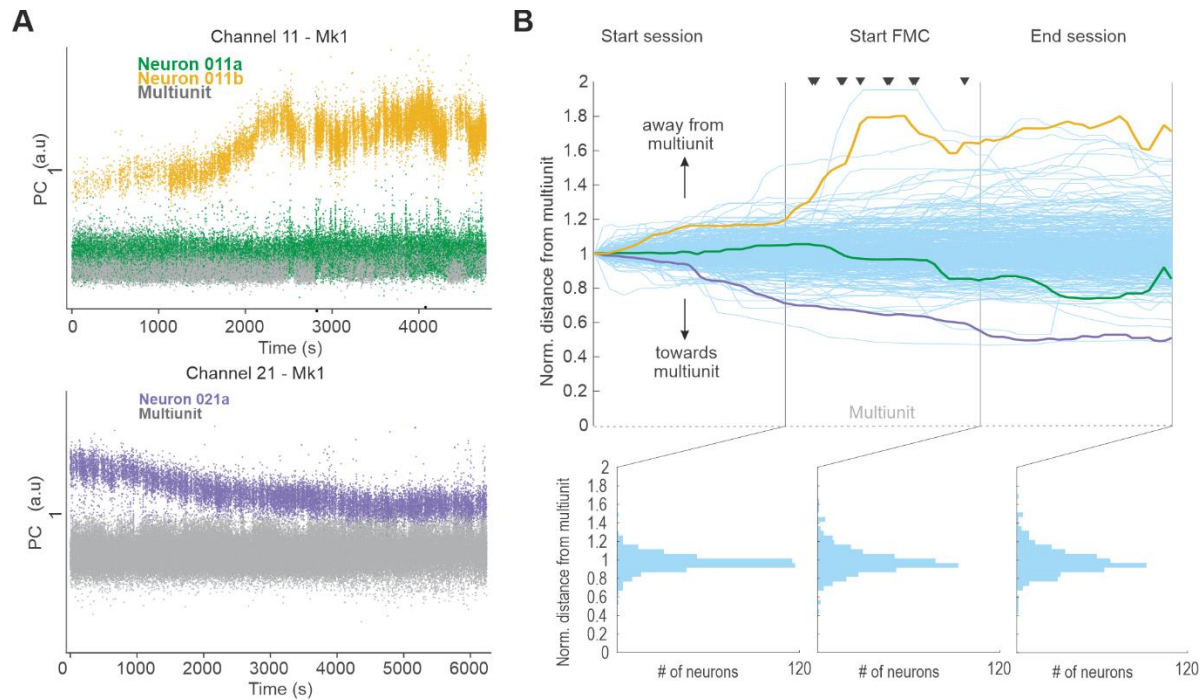
**Fig. S1. Neuro-behavioral platform enabling recording of premotor neurons.** (A) Floating Microelectrode Arrays implanted in the left and right hemispheres of Mk1 and Mk2. (B) Recording chamber design. The illustrated 8-slot model is configured with six 32-channel Omnetics connectors, with the protective cover used during freely moving neural recordings. (C) Top: Half-cover mounted on the recording chamber with the data logger and battery connected for a 128-channel recording session. Bottom: Full cover mounted and sealed. (D) Neural traces from 3 simultaneously recorded channels of Mk1 during a FMC. (E) Photograph of the NeuroEthoRoom (NER) set up for a recording session. (F) Video frame exemplifying a “drink” action in FMC (top-left) when the monkey's mouth touches the plastic spout of a syringe filled with juice; behavioral scoring of a FMC session with BORIS software (bottom-left); inter-rater reliability calculated for two scored sessions of FMC for Mk1 and Mk2 (top-right) and time lag between the same behaviors scored by the two rater (bottom-right - the black dashed line indicates the average time lag between raters).

Actions	RC/FMC	Definition of the scored event
	Both	<b>Bite:</b> The monkey opens its mouth, closes it around a piece of food (typically a morsel of fruit) given by an experimenter using a stick directly into its mouth, and then chews it; marked when food touches the mouth, corresponding to the transition between mouth opening and closure phases.
	Both	<b>Drink:</b> The monkey opens its mouth, closes it around the tip of a plastic syringe given by an experimenter directly into its mouth, and then drinks the juice; marked when the syringe touches the mouth, corresponding to the transition between mouth opening and closure phases.
	FMC	<b>Yawn:</b> The monkey opens the mouth, takes a deep inspiration followed by a brief apnea and a slow expiration, and then closes the mouth; marked on the moment of maximal mouth opening before closure starts. Start and stop of mouth opening/closure were also marked.
	Both	<b>Grasp to eat (RC):</b> The monkey grasps (with the ipsi- or contra-lateral hand) a small piece of food presented on a tray by the experimenter and brings it to the mouth; marked when the monkey's hand touches the food, corresponding to the beginning of finger flexion to secure the object. <b>Grasp to eat food from the floor (FMC):</b> The monkey grasps (with the ipsi- or contra-lateral hand) a small piece of food from the floor and brings it to the mouth; marked when the monkey's hand touches the food, corresponding to the beginning of finger flexion to secure the object. <b>Catch food from a hanging thread (FMC):</b> The monkey grasps (with the ipsi- or contra-lateral hand) a small piece of food hanging on a thread lowered from the top of the NER; marked when the monkey's hand touches the food, corresponding to the beginning of finger flexion to secure the object.
	FMC	<b>Climb:</b> Monkey performs a power grasp with the whole contralateral hand on the wooden structure; marked on the moment when the hand touches the structure, corresponding to the beginning of finger flexion to secure the grip before the arm pulling phase.
	FMC	<b>Rope climb:</b> Monkey performs a power grasp with the whole contralateral hand on the rope; marked on the moment when the hand touches the rope, corresponding to the beginning of finger flexion to secure the grip.
	FMC	<b>Scratch:</b> Brief sequence of repeated finger movements, marked on the moment when the monkey's contralateral hand makes the first contact with a body part within a cycle of repeated extension/flexion movements.
	FMC	<b>Step:</b> Monkeys' contralateral hand touches a flat surface within a sequence of walking (i.e. excluding the first and last step of a walking sequence from the analysis), corresponding to the transition between the previous swing and the subsequent stance phases.

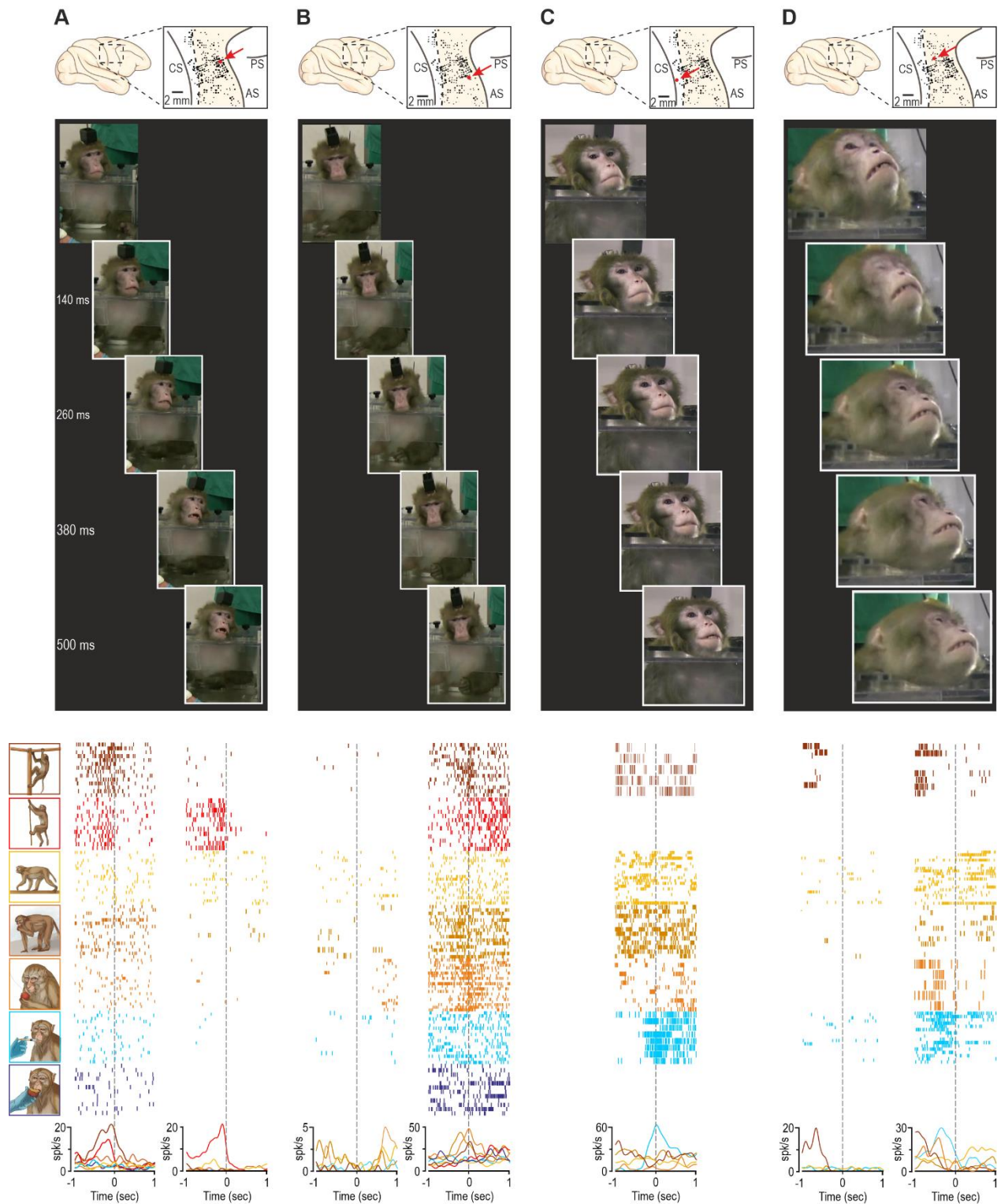
**Fig. S2. Ethogram of the investigated actions in RC and FMC and alignment events.** Mouth (blue) and forelimb (red) actions have been defined relative to the main behavioral event used as a reference for the study of the neuronal activity. Forelimb actions were separately scored for right and left limb. Examples are shown in Movie S1. See table S1 for temporal details of each action.



**Fig. S3. Recorded regions in the 4 hemispheres of Mk1 and Mk2.** The left hemispheres of both monkeys have been flipped to facilitate the comparison with the right hemispheres. The orange dashed lines indicate the putative anatomo-functional border between the primary motor cortex and the premotor cortex, defined based on the anatomo-functional evidence of previous studies (22) and the threshold of 50 ms ICMS < 25  $\mu$ A. The size of each dot represents the number of single units isolated in each site. CS, central sulcus; AS, arcuate sulcus; PS, principal sulcus. Note that the fraction of neurons modulated vs non-modulated during at least one action was not significantly different between putative primary motor (56 out of 65) and premotor (287/359) regions (Yates-corrected  $\chi^2=1,0$ ,  $p=0.32$ ).

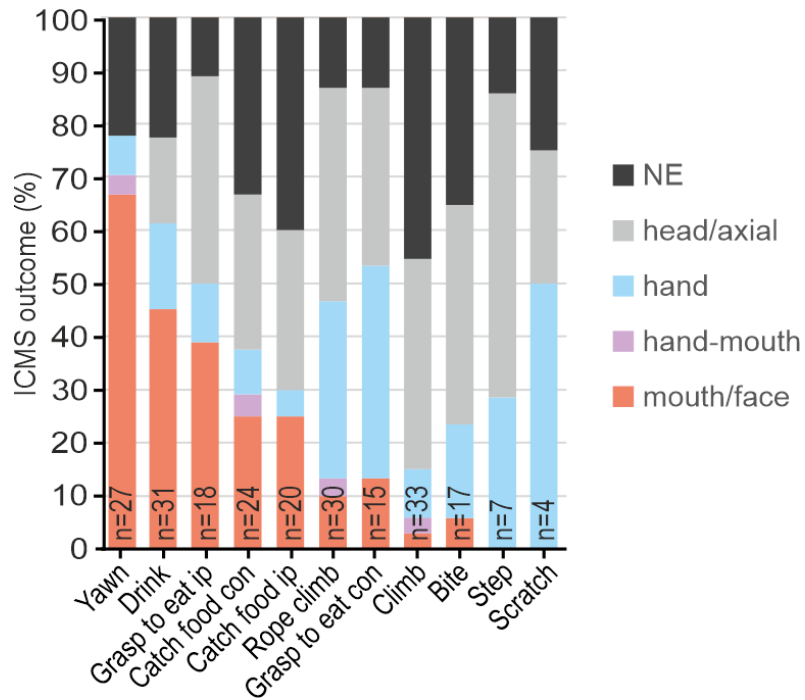


**Fig. S4. Neural recording stability along RC and FMC.** (A) Two example channels from which we recorded single unit activity. Even though the waveforms drifted along the session, they remained well isolated from the multi-unit. (B) Quantification of single unit stability along the entire session. For each neuron, we plotted the median distance computed in the first three principal component subspace between its spikes and those of the multi-unit in 1-minute bins. The resulting distance time-course was smoothed with a 10-minute moving median, linearly interpolated to a constant number of time points and normalized for the first value to make different neurons of different sessions comparable. Unstable single units that disappeared into the multi-unit during the session or appeared from it at some point, were excluded from all analyses (n=6, Mk1; n=3, Mk2).



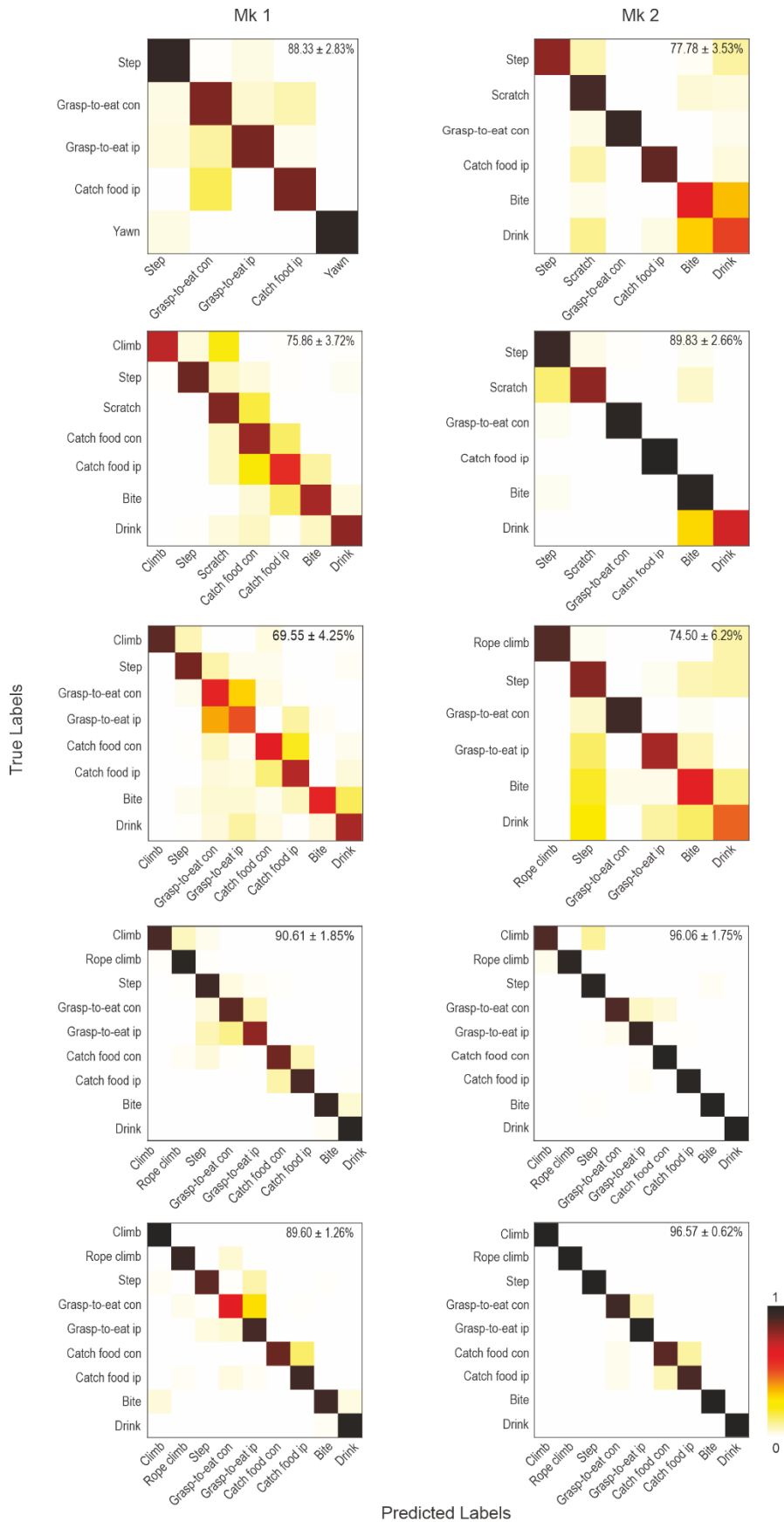
**Fig. S5. Example neurons recorded in cortical sites where ICMS evoked distinct pattern of movement.** On top of each column the map indicates the location of the sites where movements illustrated in the image sequence was evoked, and the neurons on the bottom of the figure were recorded (see Movie S2). (A) Example of a site where ICMS causes the contralateral arm to move

toward the ipsilateral side and mouth opening, and single neurons recorded in the same site showed the strongest modulation during climbing actions. **(B)** Example of a site where ICMS causes a grasping-like movement, with hand closure and concomitant wrist rotation, while neuronal activity is more strongly modulated during actions such as climbing, grasp-to-eat and catch food. **(C)** Example of a site where ICMS causes a chewing-like movement, with contraction of the contralateral oral commissure, and the single neuron recorded from the site is maximally modulated during drinking actions. **(D)** Example of a site where ICMS causes an avoidance-like movement, with a contralateral facial squint and head tilt, while neurons recorded from the same site exhibit modulation during various forelimb and facial actions.



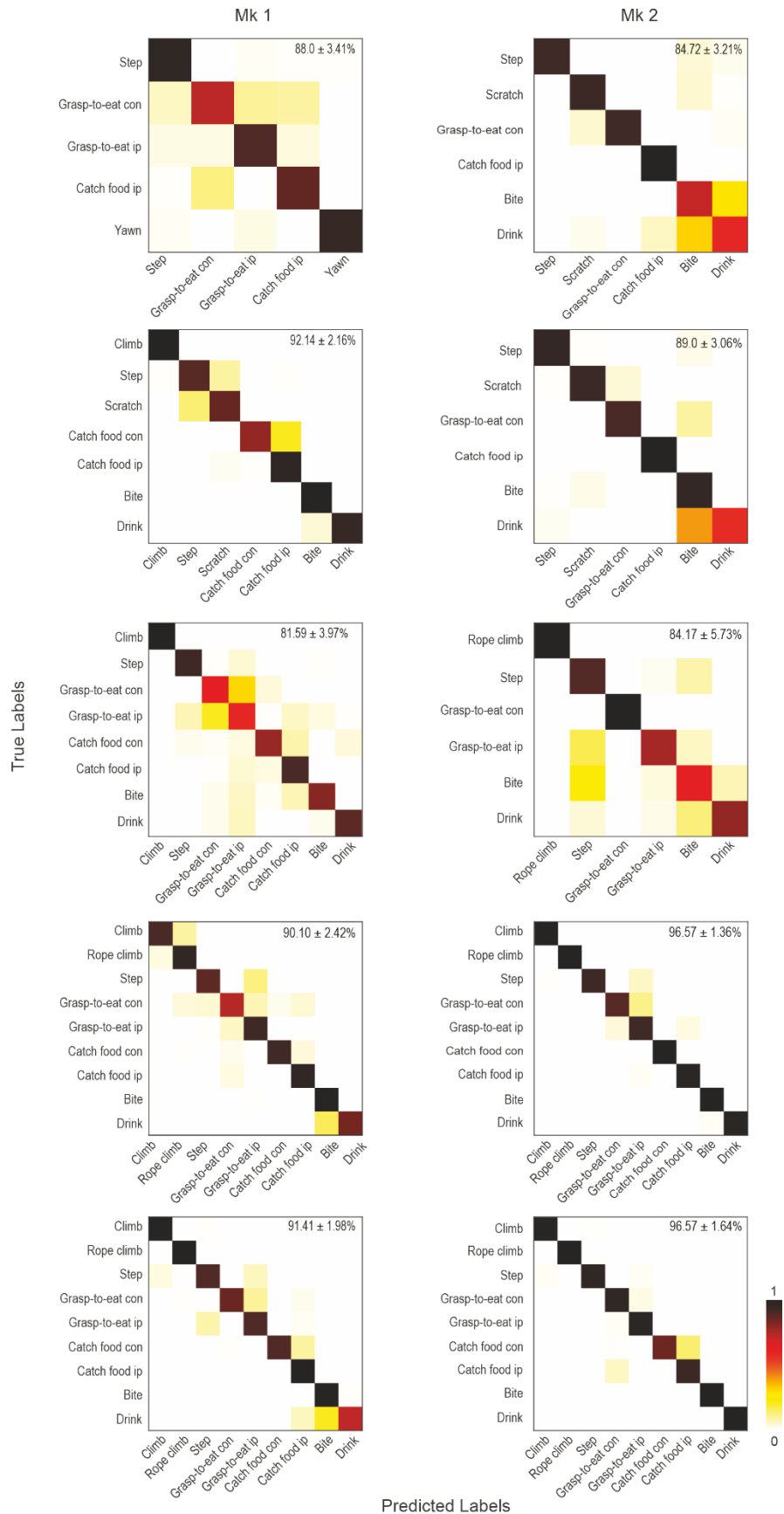
**Figure S6. Fraction of sparse coding neurons responsive to each of the tested actions recorded from non-excitable sites (NE) or sites in which ICMS triggered head/axial, hand, hand-and-mouth, or mouth/face movements.**





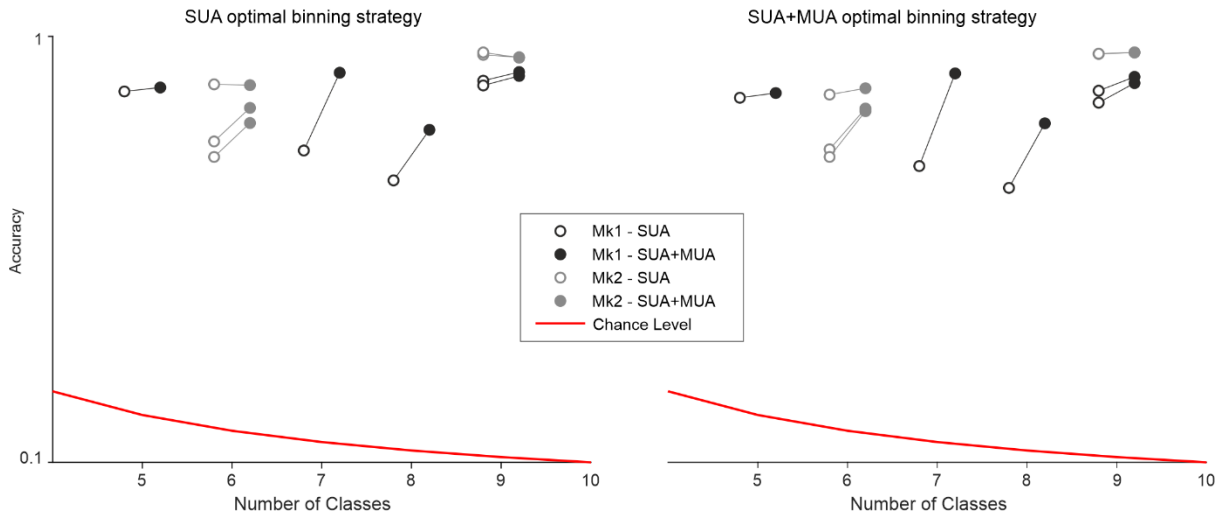
Predicted Labels

**Fig. S7. Confusion Matrices of neural decoding with single unit activity for all sessions.** Each plot illustrates the confusion matrix computed with the predictors including only single unit activity for all sessions of both monkeys. Mean and standard deviation from averaging the 10 different class-balanced partitions of the dataset are also reported. These confusion matrices are obtained using 0.5 s bins over 2.0 s of total temporal evolution.

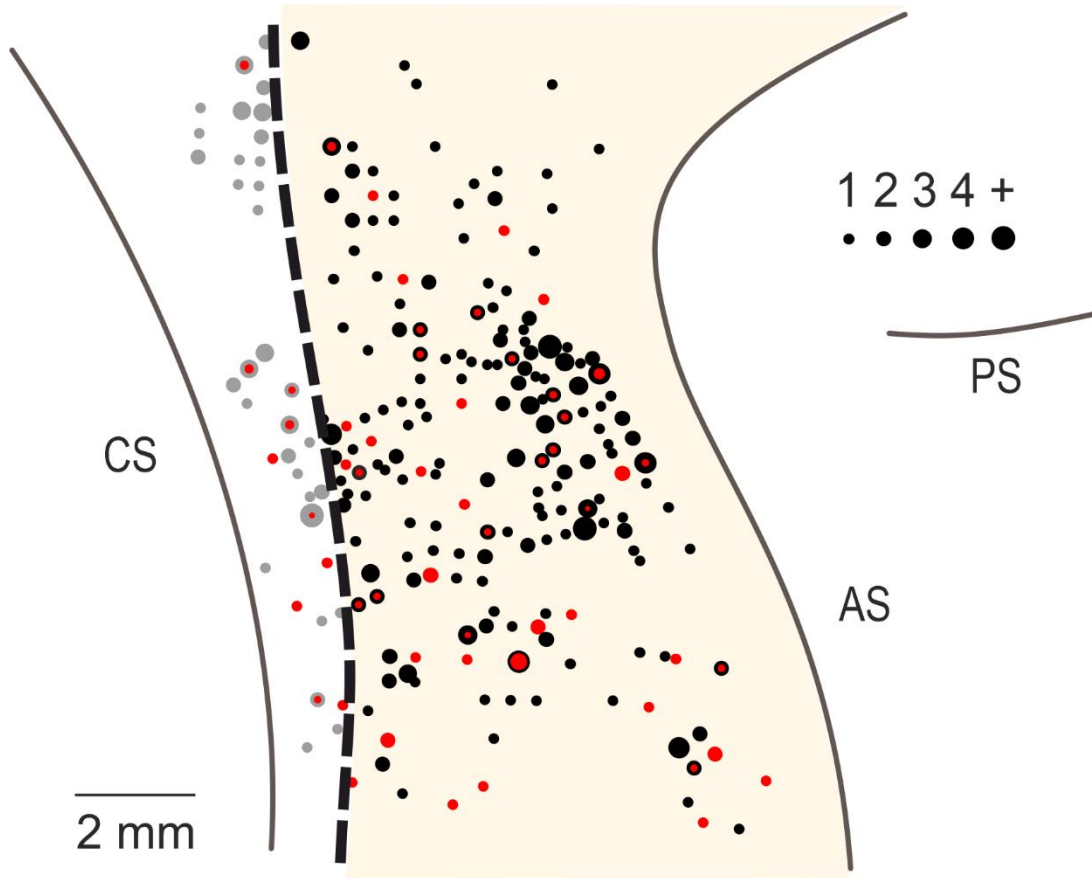


Predicted Labels

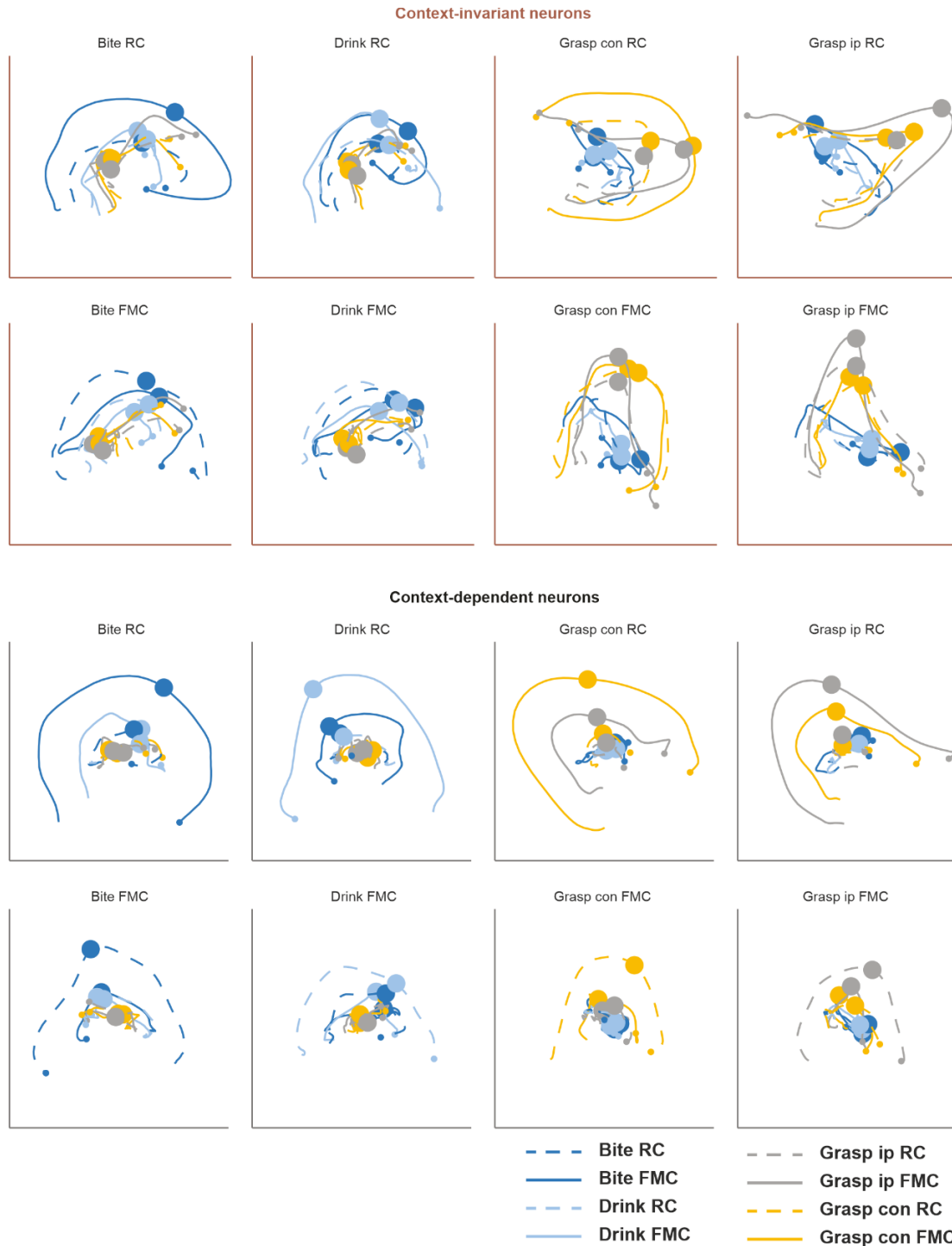
**Fig. S8. Confusion Matrices of neural decoding with single- and multi-unit activity for all sessions.** Bin width 0.5 s and 1.5 s of total temporal evolution. Other conventions as in Fig. S7.



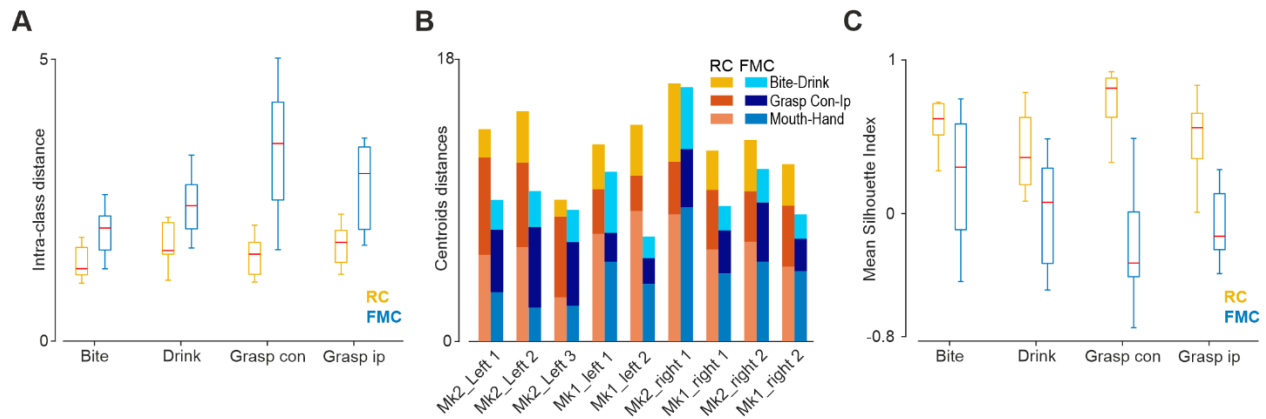
**Fig. S9. Decoding performances deriving from four different strategies for building predictors.** Scatter plots of decoding accuracies in relation to the number of classes occurring in the 10 sessions (connected dots correspond to the same session) in Mk1 (dark gray) and Mk2 (light gray). The red line indicates chance level as a function of the number of classes. The left and right panels differ for the chosen binning strategy. Left: the spike counts were obtained using the optimal parameters for the SUA (0.5 s bins, interval ranging from -1.0 to +1.0 s relative to the alignment point). Right: the spike counts were obtained using the optimal strategy for SUA+MUA (0.5 s bins, interval ranging from -0.75 s to +0.75 s relative to the alignment point).



**Fig. S10. Anatomical localization of context-invariant neurons (red).** Data have been reported on a template brain obtained by warping the four hemispheres of the two monkeys. Conventions as in Fig. 1D.



**Fig. S11. Neural trajectories of activity during actions in FMC and RC.** Neural trajectories for each of the actions ( $n=4$ ) studied across contexts ( $n=2$ ) have been projected onto the neural subspace defined by the neural activity during each action in each context. Neuronal population has been subdivided in two subpopulations of context-invariant and context-dependent neurons. The alignment between pairs of trajectories (20) corresponds to the value of each cell in the matrices of Fig. 3. Dots along the trajectories indicate the alignment point, while small dots at the extremities of the lines indicate the end of the trajectory.



**Fig. S12. Comparative measures of intra- and inter-class variability of a 3D t-SNE embedding of neural responses in RC and FMC.** (A) Intra-class variability measured for 9 sessions in terms of mean pairwise distances between all elements belonging to a specific class and context. In FMC, intra-class variability is consistently higher than in RC across all classes. (B) Inter-class variability measured in terms of centroid distances for RC and FMC in 9 sessions. Moving from bottom to top, each stacked bar represents the aggregated sum of the following distances: Mouth centroid (mean of Bite and Drink centroids) from Hand centroid (mean of Grasp Con and Grasp Ip centroids); Grasp Con centroid from Grasp Ip centroid; Bite centroid from Drink centroid. Overall, FMC has lower total inter-classes distances than RC for all sessions. (C) Silhouette Index values quantifying the clustering quality for each type of action in RC and FMC for 9 sessions.

This evidence indicates that the higher intra-class variability in FMC likely results from the combination of different nuances within each specific class, and that, together with its lower inter-class variability, FMC has higher generalizability in cross-decoding analyses compared to RC.



<b>Action</b>	<b>Definition of the event</b>	<b>Average duration in FMC (<math>\pm</math> st dev)</b>
Bite	<b>Start:</b> the monkey starts to open the mouth. <b>Stop:</b> the mouth is completely closed.	$0.65 \pm 0.17$ s
Drink	<b>Start:</b> the monkey starts to open the mouth. <b>Stop:</b> the syringe detached from the mouth.	$1.74 \pm 0.79$ s
Yawn	<b>Start:</b> the monkey starts to open the mouth. <b>Stop:</b> the moment the monkey closes the mouth.	$2.32 \pm 0.78$ s
Grasp	<b>Start:</b> the monkey starts to reach the food. <b>Stop:</b> the hand reaches the mouth.	<b>Grasp-to-eat</b> Reaching: 0.42 s Retrieving: $0.65 \pm 0.46$ s  <b>Catch food</b> Reaching: 0.69 s Retrieving: $0.71 \pm 0.66$ s
Climb	<b>Start:</b> the monkey starts to reach for the support to lift up. <b>Stop:</b> the monkey's hand lost contact with the support.	$2.15 \pm 0.45$ s
Rope climb	<b>Start:</b> the monkey starts to reach the rope. <b>Stop:</b> the monkey's hand lost contact with the rope.	$1.10 \pm 0.45$ s
Scratch	<b>Start:</b> the monkey moves the forelimb to get in contact with the body part to be scratched. <b>Stop:</b> the monkey's hand detached from the scratched body part.	$1.8 \pm 0.93$ s
Step	<b>Start:</b> the monkey's hand leaves the ground (from a previous step). <b>Stop:</b> the monkey's hand get in contact with the ground again.	$0.73 \pm 0.23$ s

**Table S1. Definition and average duration of the onset and offset of each studied action in FMC.** The values have been calculated on a subset of 15 trials per action of each monkey randomly sampled across all the sessions.

## References and Notes

1. E. A. Buffalo, J. A. Movshon, R. H. Wurtz, From basic brain research to treating human brain disorders. *Proc. Natl. Acad. Sci. U.S.A.* **116**, 26167–26172 (2019).
2. R. P. Dum, P. L. Strick, Motor areas in the frontal lobe of the primate. *Physiol. Behav.* **77**, 677–682 (2002).
3. G. Rizzolatti, G. Luppino, The cortical motor system. *Neuron* **31**, 889–901 (2001).
4. P. Cisek, J. F. Kalaska, Neural mechanisms for interacting with a world full of action choices. *Annu. Rev. Neurosci.* **33**, 269–298 (2010).
5. M. Graziano, The organization of behavioral repertoire in motor cortex. *Annu. Rev. Neurosci.* **29**, 105–134 (2006).
6. J. H. Kaas, I. Stepniewska, Evolution of posterior parietal cortex and parietal-frontal networks for specific actions in primates. *J. Comp. Neurol.* **524**, 595–608 (2016).
7. S. Kakei, D. S. Hoffman, P. L. Strick, Direction of action is represented in the ventral premotor cortex. *Nat. Neurosci.* **4**, 1020–1025 (2001).
8. M. A. Umiltà, L. Escola, I. Intskirveli, F. Grammont, M. Rochat, F. Caruana, A. Jezzini, V. Gallese, G. Rizzolatti, When pliers become fingers in the monkey motor system. *Proc. Natl. Acad. Sci. U.S.A.* **105**, 2209–2213 (2008).
9. G. Rizzolatti, M. Gentilucci, L. Fogassi, G. Luppino, M. Matelli, S. Ponzoni-Maggi, Neurons related to goal-directed motor acts in inferior area 6 of the macaque monkey. *Exp. Brain Res.* **67**, 220–224 (1987).
10. L. Bonini, F. U. Serventi, L. Simone, S. Rozzi, P. F. Ferrari, L. Fogassi, Grasping neurons of monkey parietal and premotor cortices encode action goals at distinct levels of abstraction during complex action sequences. *J. Neurosci.* **31**, 5876–5886 (2011).
11. G. Rizzolatti, J. F. Kalaska, Voluntary movement: The parietal and premotor cortex. *Princ. Neur. Sci.* **5**, 865–893 (2013).
12. V. Jovanovic, A. R. Fishbein, L. de la Mothe, K.-F. Lee, C. T. Miller, Behavioral context affects social signal representations within single primate prefrontal cortex neurons. *Neuron* **110**, 1318–1326.e4 (2022).
13. M. M. Yartsev, N. Ulanovsky, Representation of three-dimensional space in the hippocampus of flying bats. *Science* **340**, 367–372 (2013).
14. J. O’Keefe, J. Dostrovsky, The hippocampus as a spatial map. Preliminary evidence from unit activity in the freely-moving rat. *Brain Res.* **34**, 171–175 (1971).
15. B. Mimica, B. A. Dunn, T. Tombaz, V. P. T. N. C. S. Bojja, J. R. Whitlock, Efficient cortical coding of 3D posture in freely behaving rats. *Science* **362**, 584–589 (2018).
16. T. C. Foster, C. A. Castro, B. L. McNaughton, Spatial selectivity of rat hippocampal neurons: Dependence on preparedness for movement. *Science* **244**, 1580–1582 (1989).
17. C. T. Miller, D. Gire, K. Hoke, A. C. Huk, D. Kelley, D. A. Leopold, M. C. Smear, F. Theunissen, M. Yartsev, C. M. Niell, Natural behavior is the language of the brain. *Curr. Biol.* **32**, R482–R493 (2022).

18. B. A. Olshausen, D. J. Field, Sparse coding of sensory inputs. *Curr. Opin. Neurobiol.* **14**, 481–487 (2004).
19. P. Cisek, A. M. Green, Toward a neuroscience of natural behavior. *Curr. Opin. Neurobiol.* **86**, 102859 (2024).
20. Materials and methods are available as supplementary materials.
21. O. Friard, M. Gamba, BORIS: A free, versatile open-source event-logging software for video/audio coding and live observations. *Methods Ecol. Evol.* **7**, 1325–1330 (2016).
22. M. Maranesi, F. Rodà, L. Bonini, S. Rozzi, P. F. Ferrari, L. Fogassi, G. Coudé, Anatomic-functional organization of the ventral primary motor and premotor cortex in the macaque monkey. *Eur. J. Neurosci.* **36**, 3376–3387 (2012).
23. J. E. Chung, J. F. Magland, A. H. Barnett, V. M. Tolosa, A. C. Tooker, K. Y. Lee, K. G. Shah, S. H. Felix, L. M. Frank, L. F. Greengard, A fully automated approach to spike sorting. *Neuron* **95**, 1381–1394.e6 (2017).
24. M. S. A. Graziano, C. S. R. Taylor, T. Moore, Complex movements evoked by microstimulation of precentral cortex. *Neuron* **34**, 841–851 (2002).
25. O. A. Gharbawie, I. Stepniewska, J. H. Kaas, Cortical connections of functional zones in posterior parietal cortex and frontal cortex motor regions in new world monkeys. *Cereb. Cortex* **21**, 1981–2002 (2011).
26. S. A. Overduin, A. d’Avella, J. Roh, J. M. Carmena, E. Bizzi, Representation of muscle synergies in the primate brain. *J. Neurosci.* **35**, 12615–12624 (2015).
27. J. A. Gallego, M. G. Perich, S. N. Naufel, C. Ethier, S. A. Solla, L. E. Miller, Cortical population activity within a preserved neural manifold underlies multiple motor behaviors. *Nat. Commun.* **9**, 4233 (2018).
28. M. M. Churchland, K. V. Shenoy, Preparatory activity and the expansive null-space. *Nat. Rev. Neurosci.* **25**, 213–236 (2024).
29. M. Beyeler, E. L. Rounds, K. D. Carlson, N. Dutt, J. L. Krichmar, Neural correlates of sparse coding and dimensionality reduction. *PLOS Comput. Biol.* **15**, e1006908 (2019).
30. C. Y. Zhang, T. Aflalo, B. Revechakis, E. R. Rosario, D. Ouellette, N. Pouratian, R. A. Andersen, Partially mixed selectivity in human posterior parietal association cortex. *Neuron* **95**, 697–708.e4 (2017).
31. V. Raos, G. Franchi, V. Gallese, L. Fogassi, Somatotopic organization of the lateral part of area F2 (dorsal premotor cortex) of the macaque monkey. *J. Neurophysiol.* **89**, 1503–1518 (2003).
32. T. N. Aflalo, M. S. A. Graziano, Relationship between unconstrained arm movements and single-neuron firing in the macaque motor cortex. *J. Neurosci.* **27**, 2760–2780 (2007).
33. T. N. Aflalo, M. S. A. Graziano, Partial tuning of motor cortex neurons to final posture in a free-moving paradigm. *Proc. Natl. Acad. Sci. U.S.A.* **103**, 2909–2914 (2006).
34. G. Rizzolatti, R. Camarda, L. Fogassi, M. Gentilucci, G. Luppino, M. Matelli, Functional organization of inferior area 6 in the macaque monkey. II. Area F5 and the control of distal movements. *Exp. Brain Res.* **71**, 491–507 (1988).

35. M. S. A. Graziano, C. S. R. Taylor, T. Moore, D. F. Cooke, The cortical control of movement revisited. *Neuron* **36**, 349–362 (2002).
36. M. Coscia, M. J. Wessel, U. Chaudary, J. D. R. Millán, S. Micera, A. Guggisberg, P. Vuadens, J. Donoghue, N. Birbaumer, F. C. Hummel, Neurotechnology-aided interventions for upper limb motor rehabilitation in severe chronic stroke. *Brain* **142**, 2182–2197 (2019).
37. A. Nourizonoz, R. Zimmermann, C. L. A. Ho, S. Pellat, Y. Ormen, C. Prévost-Solié, G. Reymond, F. Pifferi, F. Aujard, A. Herrel, D. Huber, EthoLoop: Automated closed-loop neuroethology in naturalistic environments. *Nat. Methods* **17**, 1052–1059 (2020).
38. D. Mao, E. Avila, B. Caziot, J. Laurens, J. D. Dickman, D. E. Angelaki, Spatial modulation of hippocampal activity in freely moving macaques. *Neuron* **109**, 3521–3534.e6 (2021).
39. B. Voloh, D. J.-N. Maisson, R. L. Cervera, I. Conover, M. Zambre, B. Hayden, J. Zimmermann, Hierarchical action encoding in prefrontal cortex of freely moving macaques. *Cell Rep.* **42**, 113091 (2023).
40. M. Franch, S. Yellapantula, A. Parajuli, N. Kharas, A. Wright, B. Aazhang, V. Dragoi, Visuo-frontal interactions during social learning in freely moving macaques. *Nature* **627**, 174–181 (2024).
41. C. Testard, S. Tremblay, F. Parodi, R. W. DiTullio, A. Acevedo-Ithier, K. L. Gardiner, K. Kording, M. L. Platt, Neural signatures of natural behaviour in socializing macaques. *Nature* **628**, 381–390 (2024).
42. G. F. Elsayed, A. H. Lara, M. T. Kaufman, M. M. Churchland, J. P. Cunningham, Reorganization between preparatory and movement population responses in motor cortex. *Nat. Commun.* **7**, 13239 (2016).
43. S. J. Jerjian, M. Sahani, A. Kraskov, Movement initiation and grasp representation in premotor and primary motor cortex mirror neurons. *eLife* **9**, e54139 (2020).
44. D. Albertini, M. Lanzilotto, M. Maranesi, L. Bonini, Largely shared neural codes for biological and nonbiological observed movements but not for executed actions in monkey premotor areas. *J. Neurophysiol.* **126**, 906–912 (2021).
45. M. Lanzilotto, A. Livi, M. Maranesi, M. Gerbella, F. Barz, P. Ruther, L. Fogassi, G. Rizzolatti, L. Bonini, Extending the cortical grasping network: Pre-supplementary motor neuron activity during vision and grasping of objects. *Cereb. Cortex* **26**, 4435–4449 (2016).